Anti-Greenhouse Effect via Regulation of Surface Emissivity

Jin-Woo Cho, Sang-Soon Yoon, Eun-Joo Lee, and Sun-Kyung Kim

***Abstract*—Infrared radiation serves as a cooling channel when an emitting surface is directly exposed to the atmosphere. However, the cooling performance is restricted, or it might be transitioned to heating mode in an enclosure. In this study, we develop a design strategy to modify the surface emissivity to mitigate radiative heating in an enclosure comprising of two (i.e., a floor and a cover) gray bodies. Indoor heating experiments were performed on a copper enclosure with a view factor of 0.67, and it was demonstrated that rationally designed surfaces lowered the floor and cover temperatures by 11 °C and 2 °C when they were heated at 115 °C and 48 °C, respectively. Heat transfer simulations verified the experimental results, further indicating that the heat dissipation capability was improved with an increase in the view factor from floor to cover and the in-plane thermal conductivity of a cover. This study will provide useful guidelines for the development of passive cooling structures in an enclosure such as buildings, automobiles, electronic devices, and batteries.**

***Index Terms*—Anti-greenhouse effect, infrared photonics, passive cooling, radiative heat transfer, spectrum engineering, thermal radiation.**

I. Introduction

THERMAL management is crucial in modern devices to enhance their performance and reliability. For instance, automobiles, photovoltaics, batteries, and electronic devices should operate at a specific working temperature. Thermal management can ensure stable operation of these devices in a high-temperature environment with ambient temperatures higher than that of a critical value [1]–[4]. Similarly, thermal management is essential in residential settings to attain the thermal comfort [5], [6]. Therefore, the global demand for space cooling in industries and residential areas is rapidly growing, which is often coined as "cold crunch" [7], [8]. This trend has imposed excessive strain on electrical grids and has exacerbated carbon dioxide emissions, which is considered as a formidable social issue. Passive (i.e., zero-energy) cooling technologies based on thermal radiation has garnered immense interest as a solution for this problem because they independently act as a heat dissipation channel combined with conduction and convection [9]–[30]. Moreover, low-cost and scale-up thin films are required for passive cooling technologies, which enables to cool various structures from microscale optoelectronic devices to macroscale outdoor infrastructures [11]–[17]. Considering that the efficiencies of present optoelectronic devices such as solar cells and light-emitting diodes are inherently saturated by thermal effects [1], [3], [4], [19], [21], the implementation of an economically viable cooling channel will be a solution to break the impasse.

Previous researches conducted on radiative cooling have considered "open" systems such as building exteriors [11]–[17], solar cells [21], and dew water harvesting structures [22], where cooling products are directly exposed to the atmosphere. Radiative coolers used for these outdoor applications should be reflective in the solar spectrum (0.3–2.5 μm), and concurrently, emissive in the thermal radiation spectrum (5–30 μm). Therefore, studies on open-system radiative coolers have focused on the underlying physics required to achieve a "stepwise" absorption (or emission, according to Kirchhoff's law of thermal radiation) spectra at multiscale wavelengths. In addition, to ensure scalable fabrication, spray coating [12], roll-to-roll processing [13], and electrospinning have been intensively explored [14].

To date, the strategies developed to achieve radiative cooling have been utilized to mitigate radiative heating (i.e., the anti-greenhouse effect) in an enclosure or a "closed" system consisting of a cover and a floor, such as textiles [23]–[26], electronic skin devices [27], and automobiles [28], [29]. The inner temperature of a closed system is elevated because the thermal radiation emitted from a floor heated by external or internal thermal energy is reflected or reradiated by a cover. The design principles for open-system radiative coolers are ineffective for the mitigation of radiative heating in a closed system. For an open system, high-reflectivity metals are placed on the bottom faces of radiative coolers to thermally isolate cooling objects from solar energy. However, the metal reflectors can intensify radiative heating in a closed system because of the entrapment of thermal radiation [30].

To solve this problem, cover and floor surfaces in a closed system should be appropriately designed. For example, Heo *et al.* reported an asymmetric thermal-radiation cover that operates as a selective (i.e., 8–13 μm in wavelength) emitter on the top face and a broadband (i.e., 5–30 μm in wavelength) emitter on the bottom face in a closed system [28]. Therefore, the bottom face completely absorbs thermal energy emitted from the

Manuscript received December 15, 2021; revised January 23, 2022; accepted January 28, 2022. Date of publication February 4, 2022; date of current version February 28, 2022. This work was supported in part by the National Research Foundation of Korea through the Basic Science Research Program under Grant 2020R1A2B5B01002261 and in part by the Nano Material Technology Development Program under Grant 2021M3D1A2049865. *(Jin-Woo Cho and Sang-Soon Yoon contributed equally to this work.) (Corresponding author: Sun-Kyung Kim.)*

Jin-Woo Cho, Eun-Joo Lee, and Sun-Kyung Kim are with the Department of Applied Physics, Kyung Hee University, Yongin 17104, Korea (e-mail: hellowlsdn@khu.ac.kr; chtkdms95@khu.ac.kr; sunkim@khu.ac.kr).

Sang-Soon Yoon is with the Department of Applied Chemistry, Kyung Hee University, Yongin 17104, Korea (e-mail: ssyoon@khu.ac.kr).

Digital Object Identifier 10.1109/JPHOT.2022.3148249

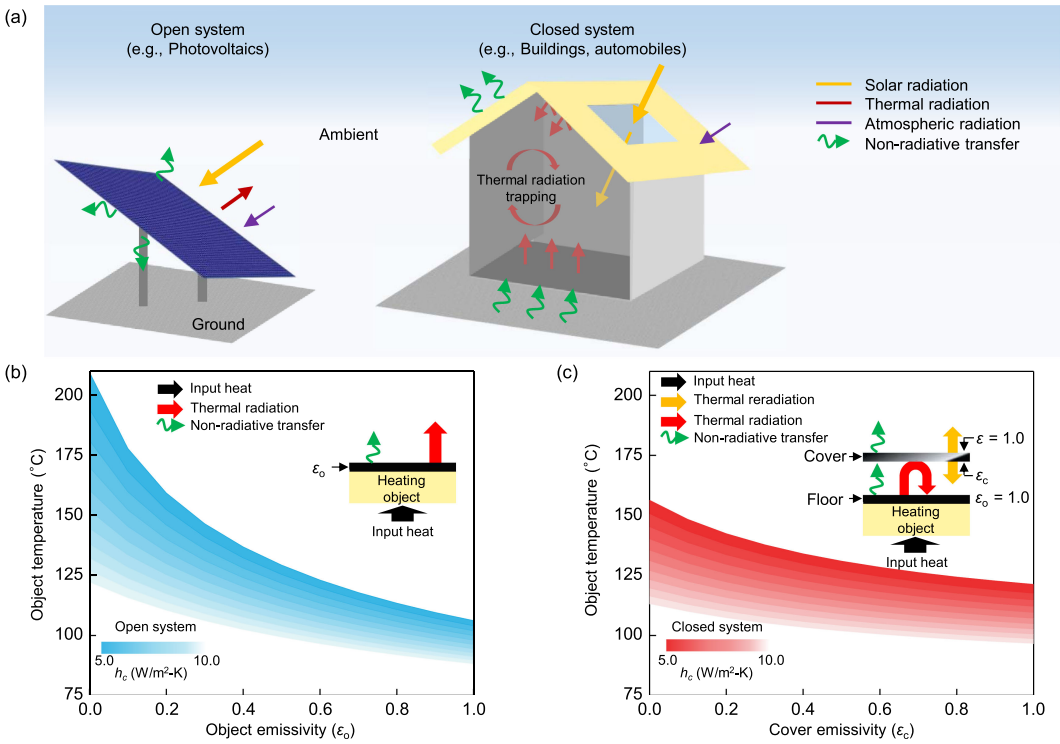

Fig. 1. (a) Schematic illustration of available heat transfer channels for open (left) and closed (right) systems. (b, c) Heat transfer simulated T_o values for the open (b) and closed (c) Systems with varying ε_o (b) and ε_c (c), respectively. For the simulations, the input heating energy, ambient temperature, and non-radiative heat-transfer coefficients (h_c) were 100 W/cm^2, 30 °C, and 5–10 W/m^2·K, respectively. (Insets) Schematic of heat transfer channels for open (b) and closed systems (c), Respectively.

floor, while the top face efficiently dissipates the accumulated thermal energy to the atmosphere through an infrared window (8–13 μm in wavelength). When the temperature of an object is equal to or lower (i.e., sub-ambient cooling) than that of the ambient temperature, a selective thermal emitter fitted into the infrared window is suitable for radiative cooling [9], [14]. This is observed because the atmospheric radiation substantially heats the heat emitter if it is inherently absorptive. Hsu *et al.* demonstrated a dual function textile that can switch between heating to cooling modes and vice versa using asymmetric surfaces with high-emissivity (ε) carbon on the top face and low-ε Cu (low-ε surface) on the bottom face [24]. The bilayer thermal emitter exhibited cooling mode when the high-ε carbon surface was exposed to the atmosphere, whereas it exhibited heating mode in the opposite configuration. Additionally, Fang *et al.* fabricated a polymer/metal elastomeric temperature modulator that can freely modulate emission, reflection, and transmission properties to switch between cooling and heating functions by exerting an external force [26].

In this study, we systemically established design rules that are essential to understand radiative cooling in a closed system. Furthermore, we demonstrated that greenhouse effect can be minimized by regulating the emissivity of cover and floor surfaces by conducting proof-of-concept experiments in a metal enclosure. We compared the thermal performance of the enclosure system using cover and floor surfaces with three different infrared (IR)-reflective, IR-transmissive, and IR-emissive properties. Finally, we investigated the effects of the view factor from floor to cover and the in-plane thermal conductivity of the cover by conducting finite element method (FEM)-based thermal simulations.

II. Results and Discussion

A. Radiative Heat Transfer in Open and Closed Systems

Fig. 1(a) illustrates the primary heat transfer channels between objects (e.g., photovoltaics or automobiles) and the atmosphere for open and closed systems. For an open system in which a cooling object directly exposed to the atmosphere, a steady-state temperature of the object (T_o) is determined by balancing the thermal energy transferred through the four channels, which are solar energy, thermal radiation from the object, atmospheric radiation, and non-radiative (i.e., conduction and convection) heat transfer [9]–[22]. T_o can be below the atmospheric temperature, provided that radiative coolers have a near-unity reflectivity in the solar spectrum. In contrast, for a closed system, the inner object (i.e., a floor) is generally hotter than that of the atmosphere due to the absorption of external solar energy or gaining internal thermal energy [23]–[30]. In addition, a closed system leads to an additional heat transfer channel which is identified as a cyclic radiative heat exchange between a floor and a cover. The thermal radiation emitted from a floor at high temperature is reflected back or it is reradiated by the cover (i.e., trapping of thermal radiation).

We conducted FEM-based thermal simulations to investigate T_o values at various emissivity values of object (ε_o) or cover (ε_c) in an open and a closed system, respectively (Fig. 1(b) and 1(c)).

For each simulation, non-radiative heat transfer coefficients (h_c) were in the range of 5–10 W/m^2·K, which corresponded to heat transfer coefficients for free convection. For an open system, T_o monotonically decreases with an increase in the value of ε_o, which accounts for conventional radiative cooling phenomenon (Fig. 1(b)). In addition, the effect of radiative cooling (i.e., the difference between the maximum (at $\varepsilon_o = 0$) and minimum (at $\varepsilon_o = 1.0$) temperatures for the same h_c) was comparatively significant at reduced h_c values, which is consistent with previously reported results [19], [21], [30]. For a closed system, we assumed that a cover surface was either absorptive or reflective for thermal radiation from a floor. Therefore, the cover did not transmit thermal radiation. If $\varepsilon_c = 0.5$, it indicated that half of the thermal radiation was absorbed, while the remaining was reflected. It should be noted that the floor surface was thermally black ($\varepsilon_o = 1$). The results of the simulations demonstrated that T_o (the floor temperature in this case) decreases with an increase in the value of ε_c because the cover expels the thermal energy transferred from the floor to the atmosphere (Fig. 1(c)). Hence, radiative heating in a closed system can be mitigated by imposing high-ε on cover surfaces, provided that the cover is not transmissive to thermal radiation.

B. Surface-Emissivity Mediated Radiative Heating

We prepared three different surfaces with IR-reflective (copper plate), IR-transmissive (low-density polyethylene (LDPE) film), and IR-emissive (black carbon-coated copper plate) spectra to investigate surface-emissivity-dependent radiative heating. The images captured using a thermal camera qualitatively revealed these distinct IR properties (Fig. 2(a)). The IR-reflective and IR-emissive samples were opaque in the thermal images, which demonstrated the thermal radiation intensity of the samples. In comparison, the IR-transmissive sample exhibited the intensity of its background. To confirm these results qualitatively, spectra of reflectance (Fig. 2(b), upper panel), transmittance (Fig. 2(b), middle panel), and absorptivity/emissivity (Fig. 2(b), lower panel) were obtained in the range of thermal radiation wavelengths (5–24 μm) using a Fourier-transform infrared (FTIR) spectrometer equipped with a gold-diffuser coated integrating sphere. The uncoated and black carbon-coated copper plates possess near-unity reflectivity and absorptivity in the range of thermal radiation spectrum (5–24 μm), respectively. In contrast, the LDPE film exhibited an average IR transmittance of 0.64, weighted by the 300-K blackbody spectrum, while retaining a null IR reflectivity. In comparison, most polymers (e.g., polyvinyl chloride, polymethylpentene, and polydimethylsiloxane) and ceramics (e.g., SiO_2, TiO_2, Al_2O_3, and Si_3N_4) possess vibration modes of functional groups and phonon-polariton resonance at characteristic wavelengths in the mid-infrared region, respectively [9], [11], [30], thus they are considered to be thermally black (i.e., IR-emissive).

Fig. 3(a) illustrates the schematics of samples used for heating experiments in open and closed systems. For an open system, the heating object was coated with or without high-ε black carbon. For a closed system, the floor was coated with the same high-ε black carbon, and it was enclosed with a cover with three different IR properties shown in Fig. 2(b). To measure T_o values

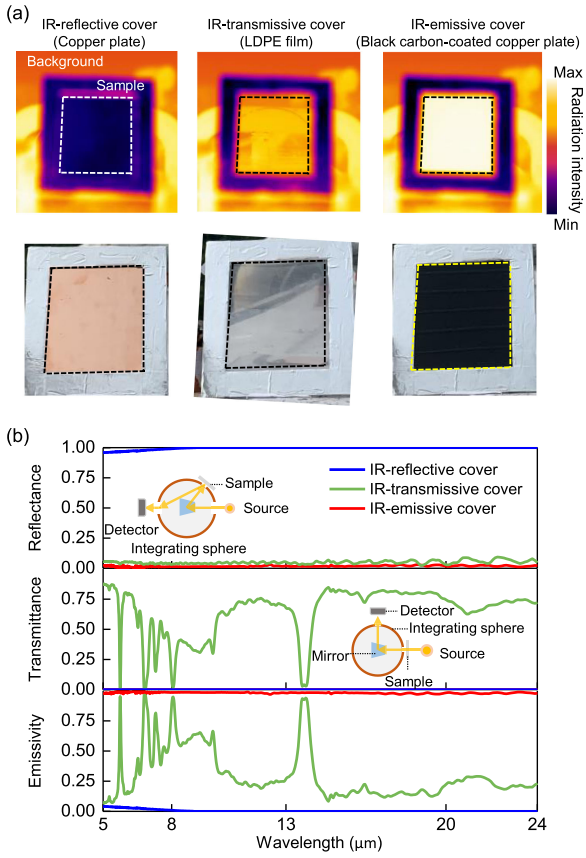

Fig. 2. (a) Images of thermal (upper panels) and visible cameras (lower panels) for the IR-reflective (copper plate), IR-transmissive (LDPE film), and IR-emissive (black carbon-coated copper plate), respectively. The scale of the bars is 5 cm. (b) Measured reflectance (upper), transmittance (middle), emissivity spectra of the samples in (a) at mid-infrared wavelengths (5–24 μm). Each inset shows the experimental setup to acquire transmittance and reflectance.

for the prepared samples, we constructed an indoor heating setup consisting of a 5 × 5 cm^2 object (floor) and a cover with a 1 cm distance (d) (Fig. 3(b)). In the present setup, the view factor from the floor to cover was 0.67. Programmed thermocouples were used to record the temporal change in temperatures of the floor and cover surfaces, while an electrical heater supplied thermal energy to the object (floor). Additional details are mentioned in Experimental Section & Methods.

Fig. 3(c) depicts the temporal changes observed in T_o (object or floor temperature for open or closed system, respectively) for each sample under the same level of electrical heating. The open system with or without the high-ε surface exhibited the lowest (103 °C) or highest T_o (116 °C), respectively, which is indicative of surface-emissivity dependent radiative cooling [8]–[24]. Conversely, T_o values in the closed system were between the highest and lowest T_o values in the open system. Particularly, the IR-reflective cover yielded the highest value of T_o (109 °C), which indicated that the maximum entrapment of thermal radiation occurred in the closed system. The IR-emissive cover exhibited a 3 °C decrease in T_o compared with that of the IR-reflective cover because it was capable of reflecting the absorbed thermal energy to the atmosphere via reradiation. However, the remaining thermal energy was reflected back to the floor, which was responsible for the higher T_o compared with that of the carbon

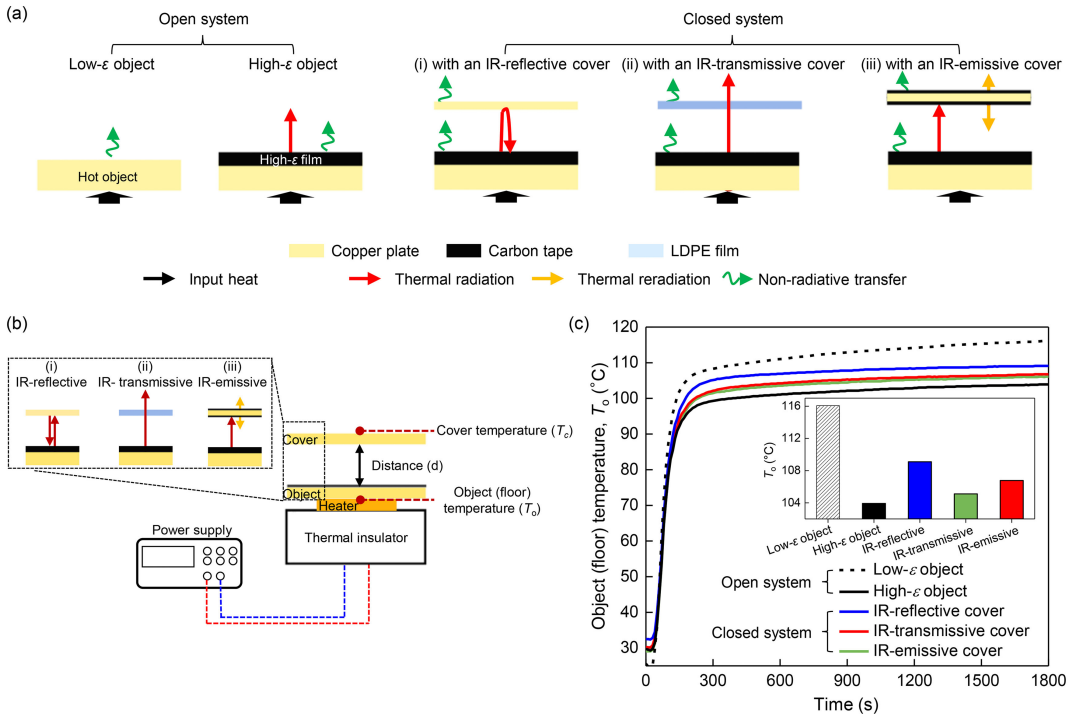

Fig. 3. (a) Conceptual schematics of open (i.e., with and without high-ε black carbon) and closed systems enclosed with (i) IR-reflective, (ii) IR-transmissive, and (iii) IR-emissive cover, respectively. The heat transfer channels are illustrated in the image. (b) Schematic of indoor radiative heating experimental setup. For the experiment, the input voltage and d values are 12 V and 1 cm, respectively. (c) The temporal change in T_o measured in open and closed systems. (Inset) T_o values measured at time 1800 s.

black-coated copper in the open system. The IR-transmissive cover exhibited the lowest value of T_o (105 °C) in the closed system because it was partially transparent at thermal radiation wavelengths (Fig. 2(b)). T_o was slightly higher than that of the carbon black-coated copper in the open system. Therefore, the most effective technique to mitigate radiative heating in a closed system is to utilize a thermally transparent material for the cover. For the same reason, IR transparent textiles can cool the human body by delivering thermal energy to the surroundings, preventing reabsorption or reradiation [23], [25].

C. Cover Emissivity Effect in Experiment

The cover of indoor devices such as displays, batteries, and electronic chips is typically composed of IR-reflective metal (e.g., aluminum and copper) [2], [28]. For an in-depth analysis of the cover emissivity-dependent radiative heating, we prepared three different configurations: an uncoated copper plate (Sample I), a single-sided (Sample II), or double-sided (Sample III) black carbon-coated copper plate (Fig. 4(a)). Similar heating experiments were conducted to obtain the temporal changes in the floor (T_o) and cover (T_c) temperatures for each sample (Fig. 4(b) and 4(c)). For the floor temperature (T_o), Sample II and Sample III exhibited a temperature drop of 8 °C and 11 °C relative to Sample I, respectively. This was observed because both the samples completely absorbed the thermal radiation emitted from the floor and transferred it to the atmosphere via convection (Sample II) or convection with thermal radiation (Sample III) (Fig. 4(b)). In contrast, in the case of cover temperature (T_c), Sample II exhibited the highest value because of its asymmetric (i.e., absorptive on the bottom face and non-emissive on the top face) optical characteristic (Fig. 4(c)). Since the cover of Sample III was colder than that of Sample II, Sample III dissipated relatively reduced thermal energy from cover to floor, which accounted for its lowest value of T_o. These proof-of-concept experiments verify the importance of high-emissivity surfaces on the top and bottom cover surfaces to mitigate radiative heating in an enclosure. The top and bottom surfaces should operate as a broadband (as opposed to selective) thermal emitter in the entire range of thermal radiation wavelengths (5–24 μm) when T_o or T_c values are significantly greater than that of atmospheric temperature [21]. The degree of temperature drop (i.e., cooling capability) can become pronounced in high-temperature applications, according to the Stefan-Boltzmann law.

D. Cover Emissivity Effect in Simulation

We conducted FEM-based thermal simulations to verify the experimental results. The indoor electric heating experiments in Figs. 3 and 4 are analogous to a heat transfer problem between two gray bodies that requires the following boundary conditions (Fig. 5(a)) [30], [31].

$$k(z)\left.\frac{dT(z)}{dz}\right|_o = P_i + F_{c\to o}P(T_c) - F_{o\to c}P(T_o) - h_{conv,\,in}(T_o - T_i), \quad (1)$$

$$-k(z)\left.\frac{dT(z)}{dz}\right|_c = F_{o\to c}P(T_o) + P(T_{atm}) - F_{c\to o}P(T_c) - h_{conv,out}(T_c - T_{atm}) + h_{conv,\,in}(T_{amb} - T_c) \quad (2)$$

For simulation, the input heating energy (P_i) was 100 mW/cm^2. The powers of thermal radiation from the floor

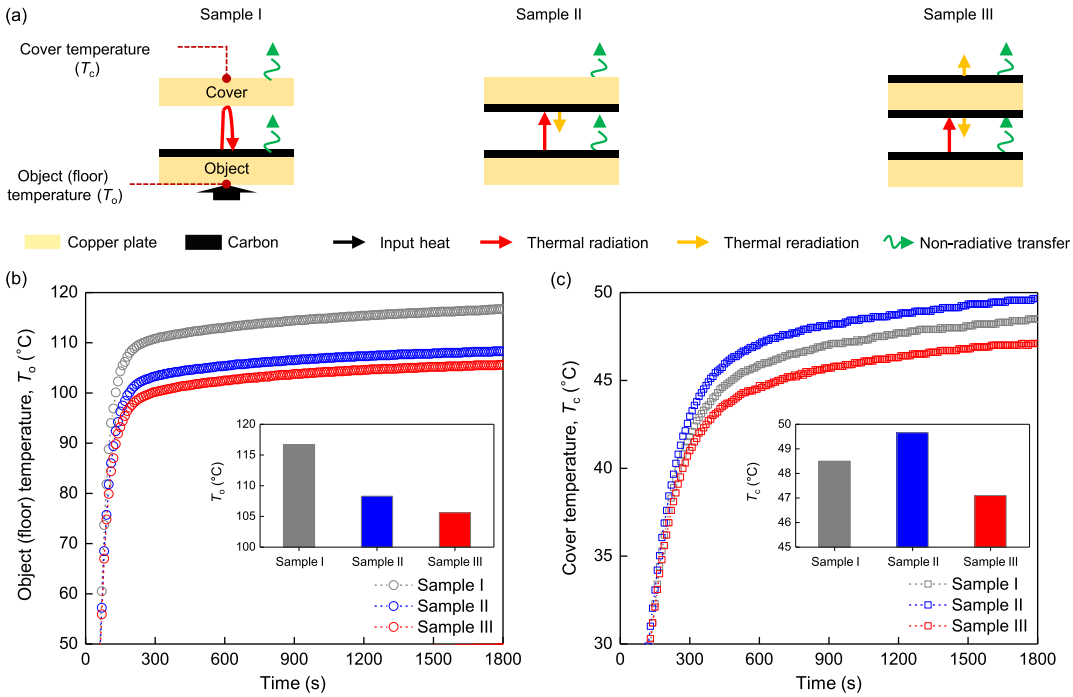

Fig. 4. (a) Comparison of the measured values in closed system samples (i.e., Samples I, II, and III). (b, c) Measurement of temporal change in T_o (b) and T_c (c) in closed systems (i.e., Samples I, II, and III), respectively. The insets in both (b) and (c) Represent T_o and T_c at 1800 s.

($P(T_o)$) and the cover ($P(T_c)$) were determined by their emissivity values. We defined T_i. as the inner temperature and set the ambient temperature (T_{amb}) to be 24 °C. The outer ($h_{conv,\ out}$) and inner thermal convection coefficients ($h_{conv,\ in}$) were 10 and 5 W/m^2·K, respectively. The thermal conductivity used for the floor and cover was 351 W/m·K, respectively, which is the same as that of copper. In general, the exchange of radiative thermal energy strongly depends upon the view factor between the floor and the cover. We defined two types of view factor: $F_{o\to c}$ from floor to object and $F_{c\to o}$ for the opposite direction. Since the structural dimensions ($5 \times 5 \times 1$ cm^3) in simulation were similar to that of in experiments, $F_{o\to c}$ was 0.67. The heat transfer channels considered are illustrated in Fig 5(a).

We simulated surface-emissivity dependent T_o for a fixed view factor (0.67) and the emissivity ($\varepsilon = 1.0$) of the top cover surface (Fig. 5(b)). For a constant ε_c, T_o steadily decreased with an increase in ε_o. Similarly, for a constant ε_o, T_o decreased with an increase in ε_c, provided that $T_o > T_c$. These simulated results underpin the experimental findings in Figs. 3 and 4 and qualitatively support the temperature drop. Moreover, they confirm that a cover with thermally black top and bottom surfaces is ideal for the mitigation of greenhouse effect in a closed system.

E. View Factor Dependent Radiative Heating

To investigate the significance of view factor in a closed system, we conducted thermal simulations with IR-emissive ($\varepsilon = 1$) or IR-reflective ($\varepsilon = 0$) cover surfaces at various values of height (h) between the floor and cover (Fig. 6(a) and 6(b)). For a fixed width (w) of 5 cm, with an increase in the value h from 0.5 to 10 cm, the view factor decreased from 0.82 to 0.05 (Fig. 6(a), inset). Accordingly, the difference in the T_o values between the IR-emissive and IR-reflective cases drastically reduced when the view factor was smaller because the heat emitted from the floor exhibited characteristics similar to that of heat emitted in an open system without a cover (Fig. 6(a)). However, we observed that the IR-emissive surfaces effectively mitigated radiative heating even at a view factor <0.2.

Finally, we investigated the effect of in-plane thermal conductivity (h_{cond}) of the cover at various view factor values (Fig. 6(b)). For these simulations, two h_{cond} values (0.033 and 351 W/m·K) were examined, which are derived from those of acrylic polymer and copper, respectively. When a cover is composed of a thermally insulating material with a low thermal conductivity, the heat is distributed non-uniformly, thereby elevating the center temperature, which is evident from the simulated results of heat map (Fig. 6(b), inset). Therefore, the difference between the temperatures of the floor and the cover becomes marginal, which mitigates radiative cooling in a closed system, irrespective of the view factor. Hence, the view factor and in-plane thermal conductivity of the cover in addition to the design of surface emissivity should be considered to suppress greenhouse effect.

III. Experimental and Methods

A. Optical Characterizations

The optical spectra in Fig. 2(b) were acquired using two different photodetectors. For visible to near-infrared wavelengths (0.3–2.5 μm), a spectrophotometer (Cary5000, Thermo Fisher) equipped with an integrating sphere was used. For mid-infrared wavelengths (2.5–24 μm), a Fourier-transform infrared (FTIR)

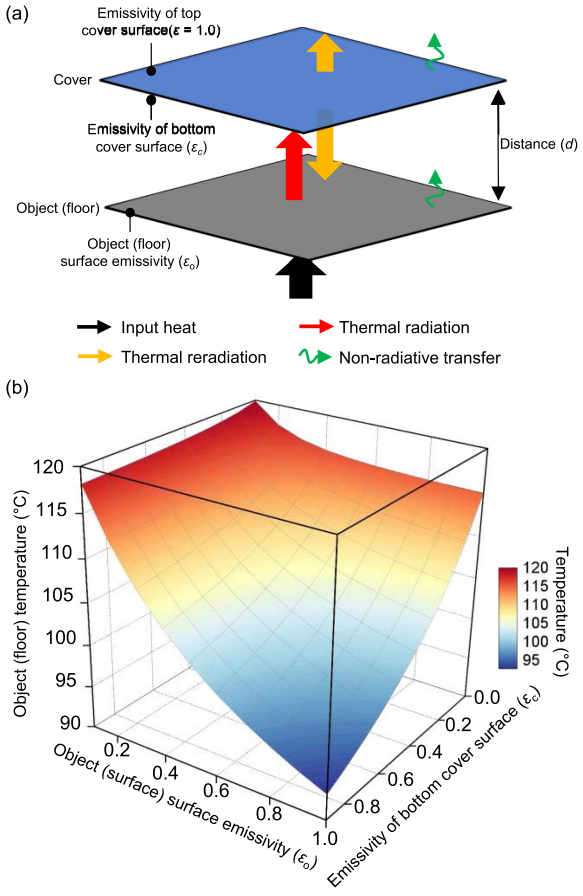

Fig. 5. (a) Schematic illustration of simulated structure and heat transfer channels. For the simulation, the object and cover were at a distance of 1 cm. The input heating energy is 100 mW/cm^2. The ambient temperature was fixed at 24 °C. The outer ($h_{\mathrm{conv,\ out}}$) and inner thermal convection coefficients ($h_{\mathrm{conv,in}}$) were 10 W/m^2·K and 5 W/m^2·K, respectively. The emissivity of top cover surface was 1.0. (b) T_{o} calculated as the function of ε_{o} and bottom cover surface of ε_{c}.

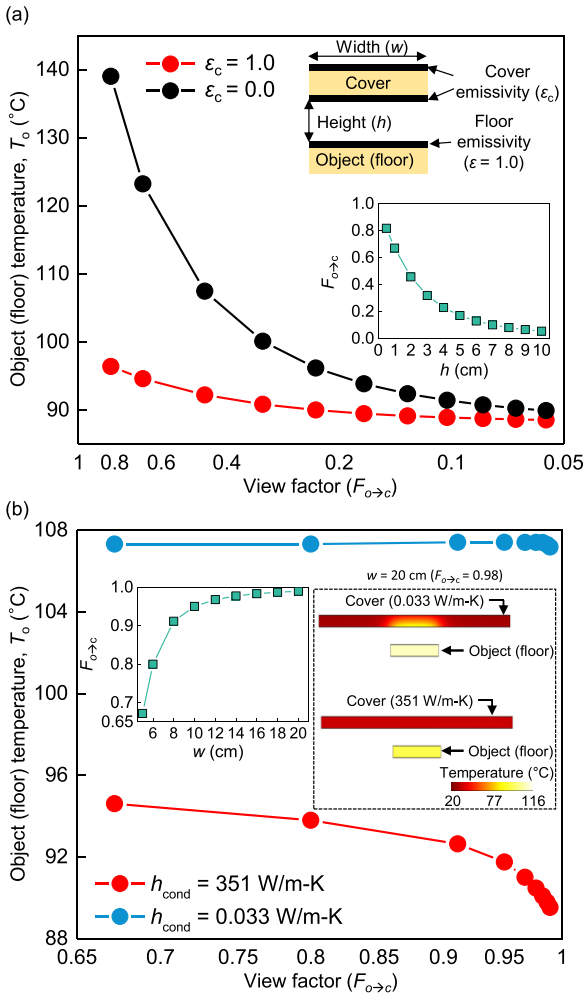

Fig. 6. (a, b) T_{o} calculated as the function of d (a) and w (b) When the cover emissivity was $\varepsilon_{\mathrm{c}} = 0$ and 1 (a) and different thermal conductivity values in the cover, i.e., 351 W/m·K and 0.033 W/m·K (b), respectively. The temperature distributions are represented in (b) at different thermal conductivity values of the cover when w is 20 cm. The insets in of (a) and (b) Represent the view factor as the function of d (a) and w (b), respectively.

spectrometer (INVENIO R, Bruker) equipped with a gold-diffuser coated integrating sphere (A562-G/Q, Thorlabs) was used.

B. Thermal Characterizations

A portable thermal imaging camera (FLIR, A655SC) was used to obtain the images in Fig. 2(a). With regard to the indoor radiative heating experiment in Figs. 3 and 4, an adhesive electric heater (HT24S, Thorlabs) was used. The temporal changes in temperatures were measured using an adhesive K-type thermocouple (SA1-K-72-SC, Omega Engineering) and recorded at an interval of 10 s on a data logger (RDXL12SD, Omega Engineering). The temperature cycling was performed through modulation of voltages using a programmable power supply (2280S, Kithley).

C. Heat Transfer Analysis

We used FEM-based thermal simulations to define T_{o} in (1) and (2). Additionally, the following heat transfer channels were considered. First, the outward radiation energy from the object is defined as

$$P(T_o) = \int d\Omega \cos\theta \int_0^\infty d\lambda I_{BB}(T_o, \lambda)\varepsilon_o(\lambda, \theta) \qquad (3)$$

In addition, the reradiation energy from the cover is written as

$$P(T_c) = \int d\Omega \cos\theta \int_0^\infty d\lambda I_{BB}(T_c, \lambda)\varepsilon_c(\lambda, \theta) \qquad (4)$$

Here $\int d\Omega = 2\pi \int_0^{\pi/2} d\theta sin\theta \int_0^{2\pi} d\phi$ is the angular integral over a hemisphere, and indicates the sample spectral and angular emissivity, respectively. For the cover of the closed system, the upper surface of the cover is exposed to the ambient surroundings. Thereby, the inward radiation energy from the ambient surroundings is

$$P(T_{atm}) = \int d\Omega \cos\theta \int_0^\infty d\lambda I_{BB}(T_{atm}, \lambda)\varepsilon_c(\lambda, \theta)\varepsilon_{atm}(\lambda, \theta) \qquad (5)$$

where $I_{BB}(T_{atm}, \lambda)$ is the spectral radiance of a blackbody at atmospheric temperature and $\varepsilon_{atm}(\lambda, \theta)$ is the atmospheric

emissivity. Here, T_{atm} was maintained at 30 °C. Moreover, we defined the view factor from the cover to object as $F_{\mathrm{o}\to\mathrm{c}}$. $F_{\mathrm{c}\to\mathrm{o}}$ was the view factor in the opposite direction. The view factors were obtained by solving the following equations [31].

$$F_{o\to c} = \frac{1}{\pi xy}\left[\ln\frac{(1+x^2)(1+y^2)}{1+x^2+y^2} + 2x\left(\sqrt{1+y^2}\arctan\frac{x}{\sqrt{1+y^2}} - \arctan x\right) + 2y\left(\sqrt{1+x^2}\arctan\frac{y}{\sqrt{1+x^2}} - \arctan y\right)\right]$$
$$x = \frac{L_x}{d}, y = \frac{L_y}{d}, \tag{6}$$

L_{x} and L_{y} are the lengths of short and long sides, respectively. Here, $L_{\mathrm{x}}(L_{\mathrm{y}})$ correspond to *w* values in Fig. 6(b). In addition, *d* is the distance between object and cover.

IV. Conclusion

In this study, we analyzed radiative heating in a closed system using various properties and structural parameters by conducting indoor electrical heating experiments and thermal simulations. We demonstrated that a cover with IR-emissive top and bottom surfaces was ideal for mitigating radiative heating, suggesting that both radiative heat transfer channels of floor to cover and cover to atmosphere contributed to "anti-greenhouse effect". FEM-based thermal simulations qualitatively supported the experimental results, further suggesting that heat dissipation rate strongly depends upon the view factor from floor to cover and the in-plane thermal conductivity of the cover. These experimental and theoretical results provide fundamental insights into the underlying principle of closed-system radiative cooling by solving heat transfer problems for two gray bodies forming an enclosure, thus enabling advanced thermal management for buildings, automobiles, electronic devices, and batteries. Moreover, harvesting sun light and maintaining specific ambient temperatures via a cost-effective, passive approach can increase crop yield by improving photosynthesis efficiency and pave the route for sustainable development toward the growing global food demand [32].

References

[1] P. Singh and N. M. Ravindra, "Temperature dependence of solar cell performance—An analysis," *Sol. Energy Mater. Sol. Cells*, vol. 101, pp. 36–45, 2012.

[2] M. Hao, J. Li, S. Park, S. Moura, and C. Dames, "Efficient thermal management of Li-ion batteries with a passive interfacial thermal regulator based on a shape memory alloy," *Nature Energy*, vol. 3, no. 10, pp. 899–906, 2018.

[3] Z. Pan, Y. Xu, Q. Hu, W. Li, H. Zhou, and Y. Zheng, "Combination cation substitution tuning of yellow-orange emitting phosphor $Mg_2Y_2Al_2Si_2O_{12}$:Ce^{3+}," *RSC Adv.*, vol. 5, no. 13, pp. 9489–9496, 2015.

[4] E. Y. Gatapova, G. Sahu, S. Khandekar, and R. Hu, "Thermal management of high-power LED module with single-phase liquid jet array," *Appl. Thermal Eng.*, vol. 184, Sep. 2021, Art. no. 116270.

[5] S. B. Sadineni, S. Madala, and R. F. Boehm, "Passive building energy savings: A review of building envelope components," *Renewable Sustain. Energy Rev.*, vol. 15, no. 8, pp. 3617–3631, 2011.

[6] X. Lu, P. Xu, H. Wang, T. Yang, and J. Hou, "Cooling potential and applications prospects of passive radiative cooling in buildings: The current state-of-the-art," *Renewable Sustain. Energy Rev.*, vol. 65, pp. 1079–1097, 2016.

[7] M. Isaac and D. P. van Vuuren, "Modeling global residential sector energy demand for heating and air conditioning in the context of climate change," *Energy Policy*, vol. 37, no. 2, pp. 507–521, 2009.

[8] J. N. Munday, "Tackling climate change through radiative cooling," *Joule*, vol. 3, no. 9, pp. 2057–2060, 2019.

[9] A. P. Raman, M. A. Anoma, L. Zhu, E. Rephaeli, and S. Fan, "Passive radiative cooling below ambient air temperature under direct sunlight," *Nature*, vol. 515, no. 7528, pp. 540–544, 2014.

[10] W. Xi, Y. Liu, W. Zhao, R. Hu, and X. Luo, "Colored radiative cooling: How to balance color display and radiative cooling performance," *Int. J. Thermal Sci.*, vol. 170, Jul. 2021, Art. no. 107172.

[11] J. Mandal *et al.*, "Hierarchically porous polymer coatings for highly efficient passive daytime radiative cooling," *Science*, vol. 362, no. 6412, pp. 315–319, 2018.

[12] X. Xue *et al.*, "Creating an eco-friendly building coating with smart subambient radiative cooling," *Adv. Mater.*, vol. 32, no. 42, 2020, Art. no. 1906751.

[13] L. Zhou *et al.*, "A polydimethylsiloxane-coated metal structure for all-day radiative cooling," *Nature Sustain.*, vol. 2, no. 8, pp. 718–724, 2019.

[14] D. Li *et al.*, "Scalable and hierarchically designed polymer film as a selective thermal emitter for high-performance all-day radiative cooling," *Nature Nanotechnol.*, vol. 16, no. 2, pp. 153–158, 2021.

[15] E.-J. Lee, J.-W. Cho, Y.-S. Kim, and S.-K. Kim, "Nanometer-optical-coating-based visibly tinted films with 24-hour sub-atmospheric passive cooling," *Opt. Lett.*, vol. 46, no. 19, pp. 5043–5046, 2021.

[16] G. J. Lee, Y. J. Kim, H. M. Kim, Y. J. Yoo, and Y. M. Song, "Colored, daytime radiative coolers with thin-film resonators for aesthetic purposes," *Adv. Opt. Mater.*, vol. 6, no. 22, 2018, Art. no. 1800707.

[17] M. Kim, D. Lee, S. Son, Y. Yang, H. Lee, and J. Rho, "Visibly transparent radiative cooler under direct sunlight," *Adv. Opt. Mater.*, vol. 2002226, pp. 1–10, 2021.

[18] B. Ko, D. Lee, T. Badloe, and J. Rho, "Metamaterial-based radiative cooling: Towards energy-free all-day cooling," *Energies*, vol. 12, no. 1, pp. 1–14, 2019.

[19] J.-W. Cho, S.-J. Park, S.-J. Park, Y.-B. Kim, Y.-J. Moon, and S.-K. Kim, "Cooling metals via gap plasmon resonance," *Nano Lett.*, vol. 21, no. 9, pp. 3974–3980, 2021.

[20] K. Zhou *et al.*, "Three-dimensional printable nanoporous polymer matrix composites for daytime radiative cooling," *Nano Lett.*, vol. 21, no. 3, pp. 1493–1499, 2021.

[21] J.-W. Cho *et al.*, "Scalable on-chip radiative coolers for concentrated solar energy devices," *ACS Photon.*, vol. 7, no. 10, pp. 2748–2755, 2020.

[22] W. Li, M. Dong, L. Fan, J. J. John, Z. Chen, and S. Fan, "Nighttime radiative cooling for water harvesting from solar panels," *ACS Photon.*, vol. 8, no. 1, pp. 269–275, 2021.

[23] P.-C. Hsu *et al.*, "Radiative human body cooling by nanoporous polyethylene textile," *Science*, vol. 353, no. 6303, pp. 1019–1023, 2016.

[24] P.-C. Hsu *et al.*, "A dual-mode textile for human body radiative heating and cooling," *Sci. Adv.*, vol. 3, no. 11, pp. 1–8, 2017.

[25] X. A. Zhang *et al.*, "Dynamic gating of infrared radiation in a textile," *Science*, vol. 363, no. 6427, pp. 619–623, 2019.

[26] H. Fang *et al.*, "A triple-mode midinfrared modulator for radiative heat management of objects with various emissivity," *Nano Lett.*, vol. 21, no. 9, pp. 4106–4114, 2021.

[27] M. H. Kang *et al.*, "Outdoor-useable, wireless/battery-free patch-type tissue oximeter with radiative cooling," *Adv. Sci.*, vol. 8, no. 10, 2021, Art. no. 2004885.

[28] S.-Y. Heo *et al.*, "A janus emitter for passive heat release from enclosures," *Sci. Adv.*, vol. 6, no. 36, 2020, Art. no. eabb1906.

[29] D. H. Kim, G. J. Lee, S. Y. Heo, I. S. Kang, and Y. M. Song, "Thermostat property of janus emitter in enclosures," *Sol. Energy Mater. Sol. Cells*, vol. 230, 2021, Art. no. 111173.

[30] J. W. Cho, S. K. Chang, S. J. Park, S. Oh, Y. Nam, and S. K. Kim, "Switching of heating and cooling modes using thermal radiation films," *Curr. Appl. Phys.*, vol. 20, no. 9, pp. 1073–1079, 2020.

[31] Y. Cengel, "Radiation heat transfer," in *Heat and Mass Transfer: Fundamentals and Applications*, 5th ed. New York, NY, USA: McGraw-Hill Education, 2014.

[32] L. Shen *et al.*, "Increasing greenhouse production by spectral-shifting and unidirectional light-extracting photonics," *Nature Food*, vol. 2, no. 6, pp. 434–441, 2021.